ACS OMEGA

http://pubs.acs.org/journal/acsodf Article

Facile Synthesis of Metal Oxide Decorated Carbonized Bamboo Fibers with Wideband Microwave Absorption

Wanxi Li,* Fang Guo, Yali Zhao, Yanyun Liu, and Yien Du

Cite This: *ACS Omega* 2022, 7, 39019−39027 Read Online

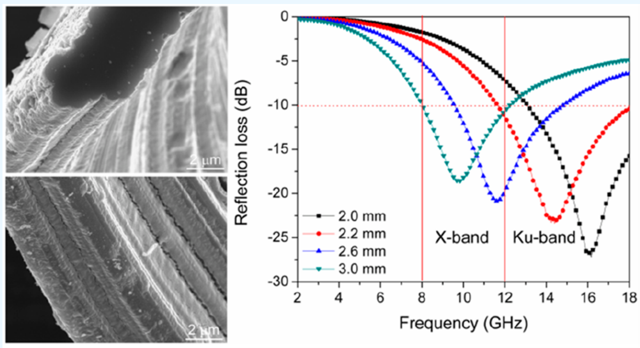

ABSTRACT: Aiming at the disadvantages of high cost, complex processes, low yield, and narrow bandwidth of carbon-based microwave absorbing materials, this paper provides a novel and efficient method for synthesizing metal oxide/carbonized bamboo fibers using renewable natural bamboo fibers as a carbon source. The results suggested that the metal oxides such as NiO and Fe_3O_4 were uniformly dispersed on the carbonized bamboo fibers and proved that the dielectric component NiO and magnetic component Fe_3O_4 can significantly improve the microwave absorption performance of the carbonized bamboo fibers. As expected, the NiO/carbonized bamboo fibers showed excellent microwave absorption performance due to the appropriate complex permittivity, high impedance matching, and attenuation coefficient. A wide effective bandwidth of 6.4 GHz with 2.2 mm thickness is achieved, covering the entire Ku-band. Remarkably, the reflection loss (RL) values less than −10 dB covered the whole X-band at a thickness of 3.0 mm. This work reveals the potential of carbonized bamboo fibers-based composite as an economic and broadband microwave absorbent and offers a new strategy for designing promising microwave absorption materials.

1. INTRODUCTION

With the wide application of electromagnetic waves, microwave absorbing materials have become the focus of attention.[1−3] There are two main applications of microwave absorbing materials. First, the absorbing materials can absorb the electromagnetic waves emitted by the radar, and reduce the probability of being detected. Second, the absorbing materials can absorb electromagnetic waves in people's living environment, and reduce signal pollution and protect people's physical and mental health. Microwave absorbing materials have increasingly high requirements for the preparation and performance of materials. Lightweight, thin thickness, strong absorption, wide frequency band, low cost, high output, and easy manufacturing are the research goals of microwave absorbing materials.[4−7] In addition, modern practical application has abundant multiple scenes, including high temperature, intense light, water flow, etc. Under the circumstances, microwave absorbing materials should be multiply functionalized with outstanding tunable properties, which bring more challenges to the research of materials.[8−10]

In recent years, carbon materials have attracted extensive attention as microwave absorbing materials because of their excellent chemical and thermal stability, excellent electrical conductivity, and low density.[11−14] Biomass is a cheap, eco-friendly, and rich renewable resource. After the carbonization of biomass, porous carbon can be obtained. Recent studies have found that porous carbon structure can not only reduce the density of materials, but also shows a strong dielectric loss, which is good for microwave absorption.[15,16] Therefore, obtaining porous carbon from biomass is a sustainable and low-cost method. It is desirable to prepare porous carbon materials from biomass under mild conditions and apply them for microwave absorption. However, due to the strong conductivity, carbon materials alone have poor impedance matching in a wide frequency range. The best method is to combine with magnetic or dielectric components to form composites, which can decrease complex permittivity and increase impedance matching.[17,18]

Recently, researchers have adjusted the microwave absorption properties of materials by adjusting the dielectric/magnetic properties.[19−21] As a p-type semiconductor, nickel oxide (NiO) has been intensively studied in electrochemical, catalytic, and magnetic applications.[22] Cao et al. have reported that NiO may significantly improve the dielectric properties of electromagnetic wave absorbing materials owing to its high permittivity, oxidation resistance, and electronic properties.[23]

Received: July 28, 2022
Accepted: October 13, 2022
Published: October 21, 2022

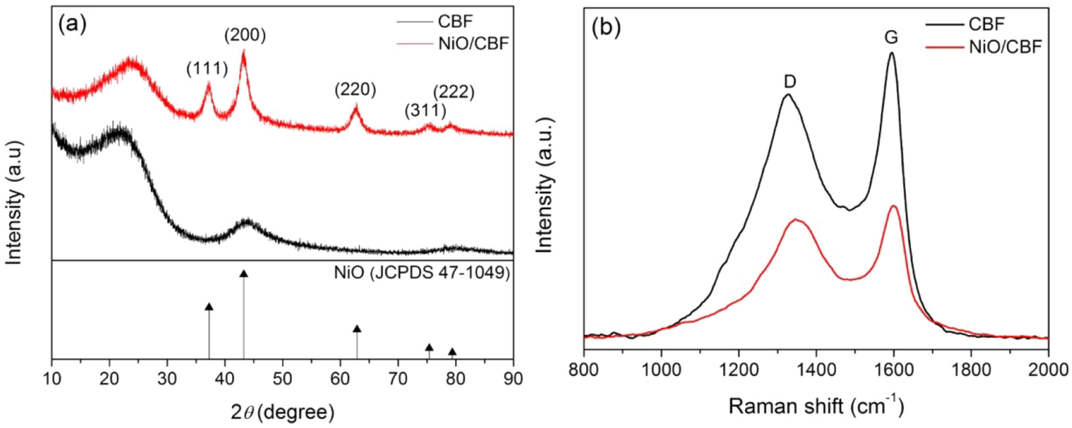

Figure 1. XRD patterns (a) and Raman spectra (b) of CBF and NiO/CBF.

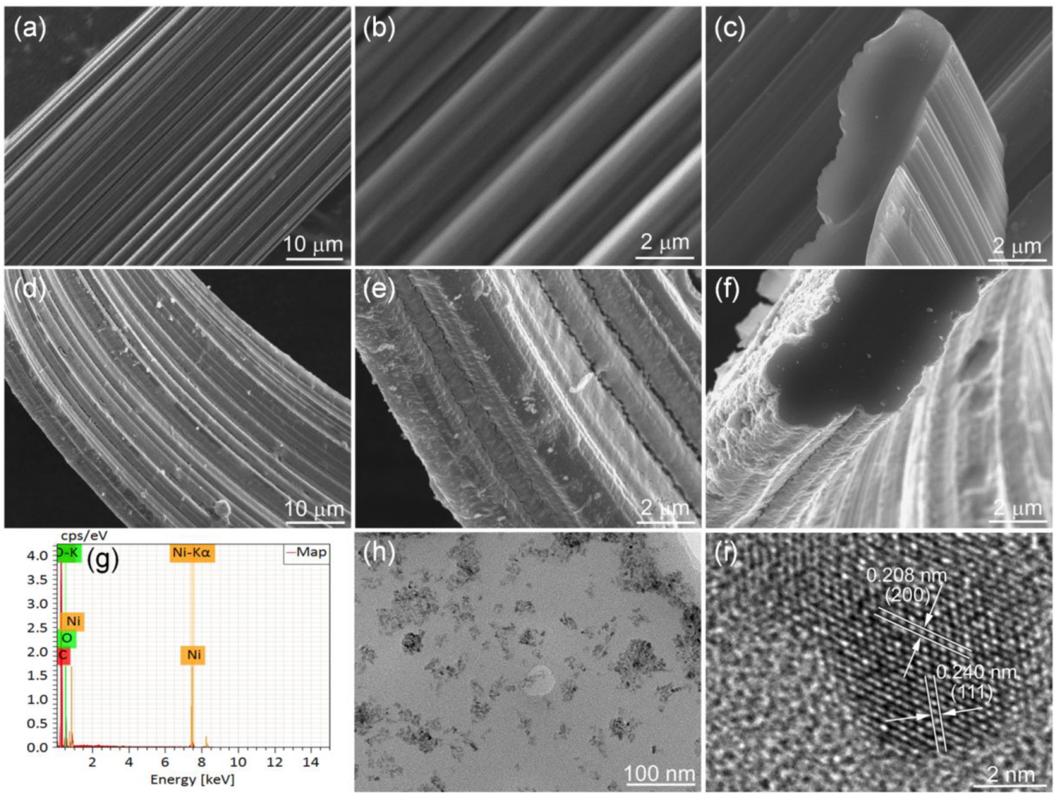

Figure 2. SEM images of CBF (a−c) and NiO/CBF (d−f); EDS pattern (g) and TEM images (h,i) of NiO/CBF.

Yao et al. have reported that NiO has the characteristics of high hole mobility, moderate dielectric loss, environmental friendliness, low cost, natural abundance, and low conductivity, which is a potential candidate for microwave absorption at gigahertz frequencies.[24] As a typical magnetic material, ferroferric oxide (Fe_3O_4) has gained much attention in electrocatalysis and energy storage.[25,26] Moreover, Fe_3O_4-based composite has become a research hotspot because it has enhanced magnetic loss, low dielectric constant, and interfacial polarization, which is conducive to impedance matching and microwave absorption.[27] Therefore, the combination of metal oxides such as NiO and Fe_3O_4 with biomass-derived porous carbon has the potential to be a lightweight, economic, and highly efficient microwave absorbent.

Bamboo fiber is one of the new friendly environment cellulose fibers extracted from natural bamboo. Herein, we prepared carbonized bamboo fibers by using cheap and readily available natural bamboo fibers as raw materials. Then, the metal oxides such as NiO and Fe_3O_4 were uniformly dispersed on the carbonized bamboo fibers by a facile impregnation method, followed by calcination. The microwave absorption properties of NiO/CBF and Fe_3O_4/CBF were studied in detail to investigate the effects of magnetic metal oxides and dielectric metal oxides on microwave absorption properties. As expected, the rich raw materials, low cost, easy manufacturing, high output, low density, good thermal stability, and wide absorption bandwidth make the microwave absorbing materials based on this work have a promising prospect as an economic, lightweight, and broadband microwave absorbent.

https://doi.org/10.1021/acsomega.2c04767
ACS Omega 2022, 7, 39019−39027

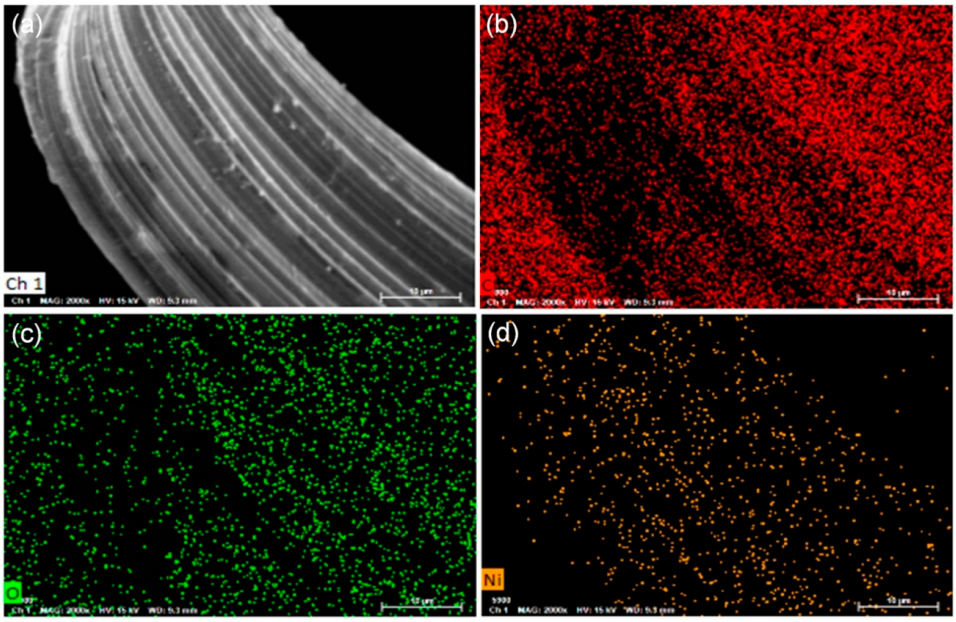

Figure 3. (a) SEM image and (b−d) elemental mapping images of NiO/CBF.

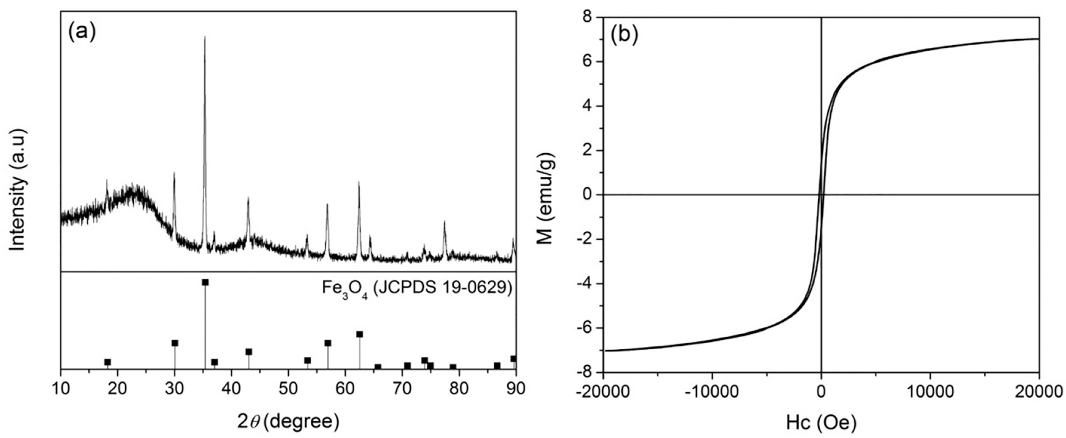

Figure 4. XRD pattern (a) and hysteresis loop (b) of Fe_3O_4/CBF.

2. RESULTS AND DISCUSSIONS

Figure 1a shows the XRD patterns of CBF and NiO/CBF. For CBF, two broad peaks at about 15°−30° and 40°−50° indicate an amorphous carbon.[28] For NiO/CBF, apart from the diffraction peaks of amorphous carbon, other diffraction peaks are consistent with NiO (JCPDS No. 47-1049), proving that the $Ni(NO_3)_2$ is decomposed to NiO after calcination treatment in the muffle furnace. Figure 1b shows the Raman spectra of CBF and NiO/CBF. Two broad peaks can be seen at about 1350 and 1588 cm^{-1}, corresponding to the D-band and G-band of carbon, respectively. The D-band can be attributed to the sp^3 defects in carbon, while the G-band represents the sp^2 structure of graphite.[29] The intensity ratio of the D-band and G-band (I_D/I_G) can be used to evaluate the graphitization degree of carbon. For CBF and NiO/CBF, the values of I_D/I_G are 0.92 and 0.97, respectively. The NiO/CBF has a higher I_D/I_G, indicating the decrease of the graphitization degree and the reduction of the conductivity of the material. In addition, after the CBF is loaded with NiO, the intensity of the D-band and G-band decreases, which is consistent with the XRD results.

Figure 2a−c shows the SEM images of CBF. The surface of the carbonized bamboo fibers is smooth, and there are regular stripes along the fiber direction. The fiber has a diameter of about 50 μm and a thickness of 3 μm. Figure 2d−f shows the SEM images of NiO/CBF, and the surface of the fiber becomes rough, indicating that the NiO particles were successfully loaded on CBF. Figure 2g shows the EDS pattern of NiO/CBF, from which the NiO/CBF consists of C, O, and Ni elements. Figure 2h shows the TEM images of NiO/CBF. The NiO nanoparticles are uniformly dispersed on the carbonized bamboo fibers. Figure 2i shows the HRTEM image of the NiO nanoparticles in NiO/CBF, and the size of the NiO nanoparticles is about 5 nm. Two kinds of lattice fringes can be identified. The crystal plane spacing is 0.208 and 0.240 nm, respectively, corresponding to the (200) and (111) crystal planes of NiO. In conclusion, the XRD pattern, SEM, and TEM images proved the successful synthesis of NiO/CBF composites.

To illuminate the distribution of the elements of NiO/CBF, the corresponding elemental mapping was characterized by EDS and shown in Figure 3. It can be seen that the Ni and O

https://doi.org/10.1021/acsomega.2c04767
ACS Omega 2022, 7, 39019−39027

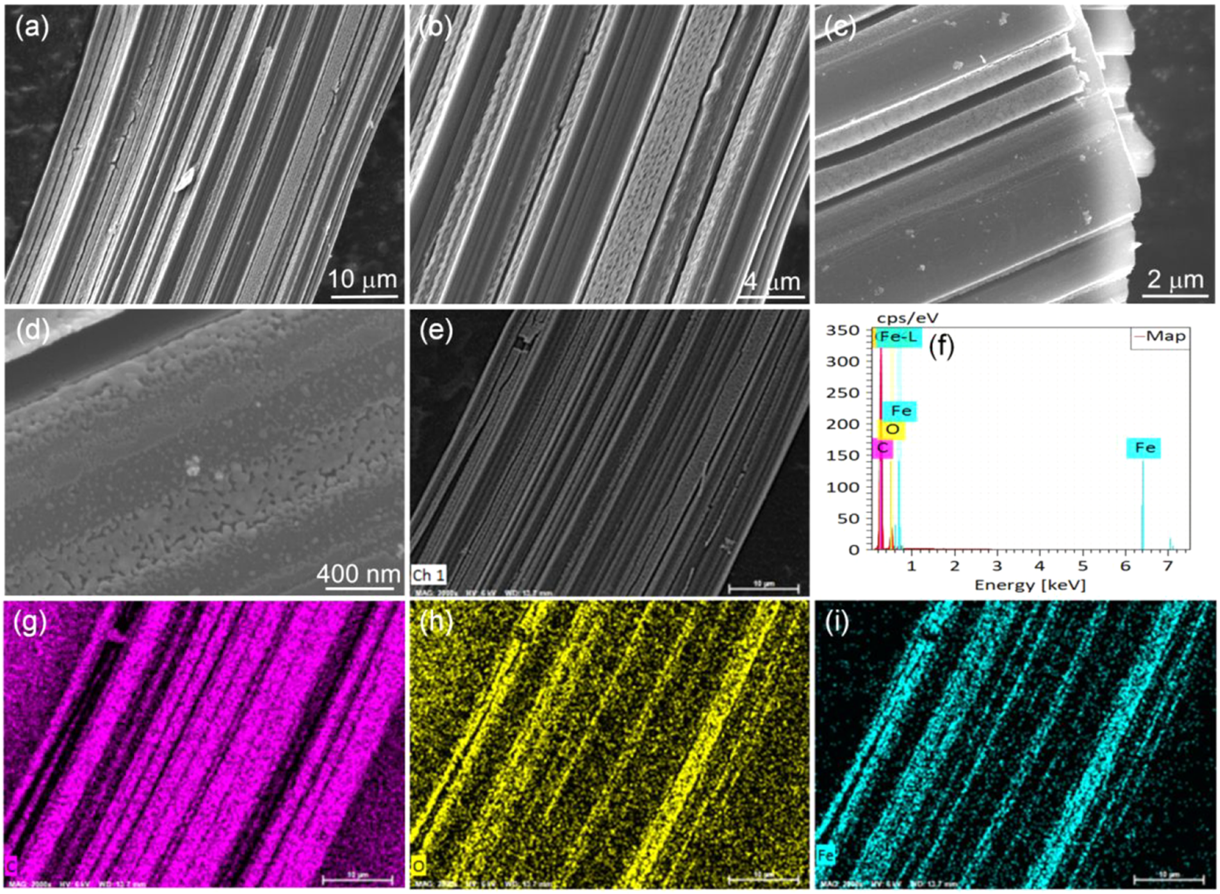

Figure 5. (a−e) SEM images, (f) EDX spectra, and (g−i) elemental mapping images of Fe_3O_4/CBF.

elements are displayed in different colors and evenly distributed on the carbonized bamboo fiber.

Figure 4a shows the XRD pattern of Fe_3O_4/CBF. The broad diffraction peaks at about 15°−30° and 40°−50° indicate an amorphous carbon. All other diffraction peaks are consistent with the diffraction peaks of Fe_3O_4 (JCPDS No. 19-0629). The narrow and sharp diffraction peaks show that the Fe_3O_4 has good crystallinity. The XRD result shows that the facile calcination method can realize the coexistence of Fe_3O_4 and carbonized bamboo fibers. Figure 4b displays the hysteresis loop of Fe_3O_4/CBF at room temperature, and the hysteresis loop shows a typical ferromagnetic behavior with a saturation magnetization (M_S) of 7.02 emu/g. The value of M_S is much lower than the pure Fe_3O_4, which is attributed to nonmagnetic carbonized bamboo fibers. Figure 5a−d shows the SEM images of Fe_3O_4/CBF at different magnifications. From the SEM images, we can observe that the Fe_3O_4 is tightly attached to the surface of the carbonized bamboo fibers. Figure 5f−i shows the element diagram and elemental mapping images of Fe_3O_4/CBF in Figure 5e. It shows that the Fe_3O_4/CBF is mainly composed of C, O, and Fe elements, and the Fe and O elements are evenly distributed along the carbonized bamboo fiber.

To quantitatively analyze the loading amount of NiO and Fe_3O_4 on the carbonized cotton fibers, we studied the TG curves of NiO/CBF and Fe_3O_4/CBF in air atmosphere (Figure. 6). Since the carbonized cotton fiber can be burned completely in an air atmosphere at high temperature, the residual product of NiO/CBF is NiO. It is estimated that the loading amount of NiO nanoparticles on carbonized bamboo fibers is 9.5 wt %. For Fe_3O_4/CBF, the Fe_3O_4 can be transformed into α-Fe_2O_3 under an air atmosphere. The content of the Fe_3O_4 on the carbonized cotton fibers can be calculated by the following formula[30]

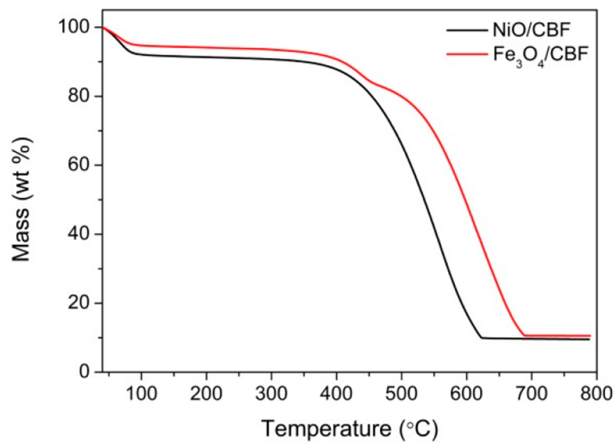

Figure 6. TG curves of NiO/CBF and Fe_3O_4/CBF in air atmosphere.

$$\text{wt \%}\ M = 2M(Fe_3O_4) \times R/3M(\alpha - Fe_2O_3) \tag{1}$$

where R represents the residual weight percentage, $M(Fe_3O_4)$ and $M(\alpha\text{-}Fe_2O_3)$ stand for the molecular weights of Fe_3O_4 and α-Fe_2O_3, respectively. According to the above analysis, the loading amount of Fe_3O_4 on the carbonized cotton fibers is

https://doi.org/10.1021/acsomega.2c04767
ACS Omega 2022, 7, 39019−39027

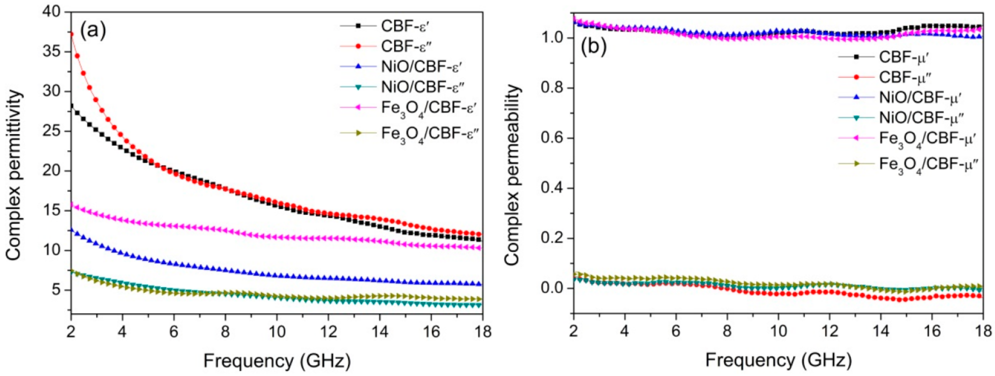

Figure 7. Frequency dependence of (a) complex permittivity and (b) complex permeability of CBF, NiO/CBF, and Fe_3O_4/CBF.

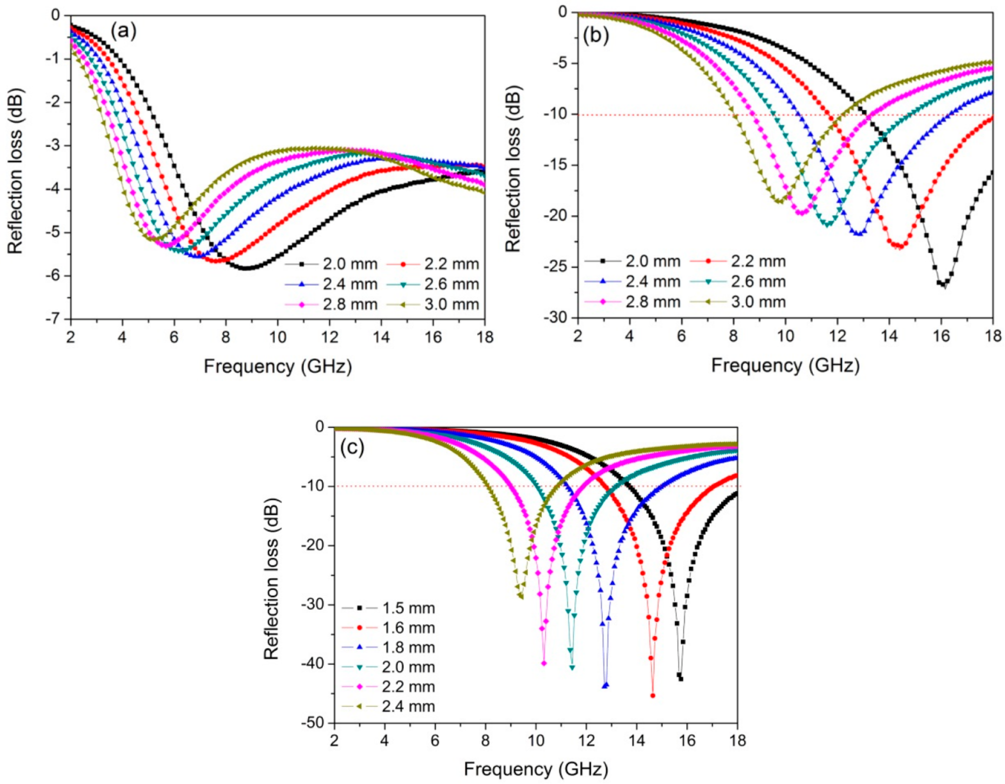

Figure 8. RL curves of (a) CBF, (b) NiO/CBF, and (c) Fe_3O_4/CBF with different thicknesses.

10.2 wt %. In addition, the NiO/CBF and Fe_3O_4/CBF have small weight loss below 400 °C, displaying good thermal stability.

According to the principle of electromagnetic energy conversion, the reflection and attenuation characteristics of electromagnetic absorbing materials are determined by the complex permittivity ($\varepsilon_r = \varepsilon' - j\varepsilon''$) and the complex permeability ($\mu_r = \mu' - j\mu''$). The ε' and ε'' represent the capacity and loss of electric field energy, while the μ' and μ'' express the capacity and loss of magnetic energy.[31,32] Generally, an excellent electromagnetic absorbent must meet two requirements: (1) Good impedance matching enables electromagnetic waves to fully propagate into the absorbent, avoiding strong reflection. Specifically, if the complex permittivity is too large, most incident electromagnetic waves will be reflected from the material surface, so the impedance matching is poor. (2) Good attenuation performance ensures the rapid attenuation of incident electromagnetic waves, which depends on the electromagnetic loss capacity. Figure 7a shows the complex permittivity of CBF, NiO/CBF, and Fe_3O_4/CBF. It is clear that the values of ε' decrease from 28.18, 12.58, and 15.78 to 11.15, 5.70, and 10.23, respectively, while the values of ε'' decrease from 37.22, 7.27, and 7.47 to 11.97, 3.16, and 3.93, respectively. The ε' and ε'' of CBF are significantly higher than NiO/CBF and Fe_3O_4/CBF. According to the free electron theory, $\varepsilon'' = 1/(2\pi\rho f\varepsilon_0)$, where ρ is the electric resistivity, f is the electromagnetic wave frequency, and ε_0 is the permittivity of free space.[33,34] The high ε'' means a low electric resistivity and high electrical conductivity, and the loading of NiO and Fe_3O_4 can decrease the electrical conductivity. Figure 7b shows the complex permeability of CBF, NiO/CBF, and Fe_3O_4/CBF. The μ'' values follow the order of Fe_3O_4/CBF > NiO/CBF > CBF, indicating that the introduction of NiO and Fe_3O_4 can increase magnetic energy loss. Moreover, the

https://doi.org/10.1021/acsomega.2c04767
ACS Omega 2022, 7, 39019−39027

Fe_3O_4/CBF has the highest magnetic energy loss due to the magnetism of Fe_3O_4.

Generally speaking, the microwave absorption performance can be expressed by the reflection loss (RL) curve. RL below −10 dB means that more than 90% of the incident microwave is absorbed, and the effective bandwidth is the width of the frequency range when the RL equals to −10 dB. Based on the above-measured ε_r and μ_r, the RL can be deduced by transmission line theory as follows[35,36]

$$Z_{in} = (\mu_r/\varepsilon_r)^{1/2} \tanh[j(2\pi fd/c)(\mu_r\varepsilon_r)^{1/2}] \quad (2)$$

$$\mathrm{RL\ (dB)} = 20 \log|(Z_{in} - Z_0)/(Z_{in} + Z_0)| \quad (3)$$

where Z_{in} is the input characteristic impedance of the absorbent, f is the frequency of the electromagnetic wave, d is the thickness of absorbent, c is the speed of light in free space, and Z_0 is the characteristic impedance of free space.

Figure 8 shows the RL curves of CBF, NiO/CBF, and Fe_3O_4/CBF. For CBF, the minimum RL is only −5.83 dB, and the effective bandwidth is 0. For NiO/CBF, the minimum RL is −27.18 dB, and the effective bandwidth can reach 6.4 GHz (11.6−18 GHz) with a thickness of 2.2 mm, covering the whole Ku-band (12−18 GHz); when the thickness increases to 3.0 mm, the effective bandwidth is 4.2 GHz (8−12.2 GHz), covering the whole X-band (8−12 GHz). For Fe_3O_4/CBF, when the thickness is 1.6 mm, the effective bandwidth is 4.3 GHz (12.8−17.1 GHz) with a minimum RL of −45.34 dB. The effective bandwidth is also 4.3 GHz (13.7−18 GHz) with a thickness of 1.5 mm. In addition, as shown in Figure 8, it can be seen that the RL peak moves to the low-frequency region with increasing thickness. What is more, the RL peak shifts to the high-frequency region by decreasing the complex permittivity under the same thickness by comparing these three samples, and this can be explained by the geometric effect.[37,38] The thickness (t) of the absorbent follows the 1/4 wavelength model: $t = n\lambda_0/4(|\mu_r||\varepsilon_r|)^{1/2} = nc/4f(|\mu_r||\varepsilon_r|)^{1/2}(n = 1,3,5,\cdots)$, and the matching frequency is inversely proportional to the thickness and complex permittivity. Thus, it is understandable that the optimal RL moves to the high thickness with decreasing the complex permittivity for these three samples. In summary, the NiO/CBF and Fe_3O_4/CBF show enhanced microwave absorption performance with wider effective bandwidth and stronger RL value compared with CBF. Moreover, the NiO/CBF displays very attractive microwave absorption performance in the entire Ku-band and X-band, which can meet the multifunctional needs of microwave absorbing materials. Compared with traditional microwave absorbents, the density of NiO/CBF is very low due to the use of carbonized bamboo fibers. Compared with other carbon-based microwave absorbing materials (shown in Table 1), the NiO/CBF has a wider effective bandwidth.[39−46] The rich natural source, simple preparation method, and wide absorption bandwidth make NiO/CBF has a broad application prospect as an economic, lightweight, and broadband microwave absorbent.

Impedance matching and attenuation coefficient are two crucial factors that determine the microwave absorption characteristics of absorbent. The closer the characteristic impedance of the absorbent is to 1 (Z_{im} value of air), the more incident microwave can be transmitted to the absorbent, which means that the impedance matching of the material is better. Research has found that the μ_r value is much lower than the ε_r value for carbon materials. Therefore, The decrease of the ε_r value can increase the characteristic impedance and improve the impedance matching of the material.[47,48] On the contrary, the higher the attenuation coefficient, the greater the electromagnetic loss. The attenuation coefficient and characteristic impedance of the absorbent can be estimated according to[49,50]

$$\alpha = \frac{\sqrt{2}\pi f}{c}\sqrt{\varepsilon''\mu'' - \varepsilon'\mu' + \sqrt{(\mu'^2 + \mu''^2)(\varepsilon'^2 + \varepsilon''^2)}} \quad (4)$$

$$Z_{im} = \sqrt{\mu_r/\varepsilon_r} = \sqrt{\sqrt{(\mu'^2 + \mu''^2)/(\varepsilon'^2 + \varepsilon''^2)}} \quad (5)$$

Figure 9 shows the attenuation coefficient and characteristic impedance of CBF, NiO/CBF, and Fe_3O_4/CBF. It can be seen from Figure 9a that the attenuation coefficient of CBF is greater than NiO/CBF and Fe_3O_4/CBF, showing a higher electromagnetic loss, which originated from the high conductivity and high conductive loss of CBF. However, the characteristic impedance of CF is much smaller than NiO/CBF and Fe_3O_4/CBF (Figure 9b), indicating poor impedance matching, which is not conducive to the transmission and loss of electromagnetic waves. This is because the complex permittivity of CBF is too high so that the incident electromagnetic wave can be strongly reflected from the surface of the material. Meanwhile, the increase of complex permeability for NiO/CBF and Fe_3O_4/CBF can promote magnetic-dielectric synergy and improve impedance matching.[51] In addition, the interfacial polarization loss caused by multi-interfaces between carbonized bamboo fibers and metal oxide is favorable for dielectric loss, resulting in the improved microwave absorption performance.[52,53] For NiO/CBF, the attenuation coefficient is slightly smaller than that of CBF and Fe_3O_4/CBF, but the characteristic impedance is the highest in the range of 2−18 GHz. The high characteristic impedance is mainly because the complex permittivity of NiO/CBF is moderate, and the NiO/CBF has a relatively low ε' value and a relatively high ε'' value, which is beneficial to the impedance matching. The balance of impedance matching and electromagnetic loss eventually leads to low reflection coefficient and excellent microwave absorption performance. We have also discussed the effect of the filler content of NiO/CBF on microwave absorption performance. When decreasing the filler content of NiO/CBF in the paraffin to 33 wt %, the microwave

Table 1. Microwave Absorption Performances of Some Reported Carbon-Based Absorbents

sample	filling rate (wt %)	effective absorption bandwidth (GHz)	references
MOF-Derived Porous Co/C Nanocomposites	60	5.8	[39]
Fe_3O_4/multiwall carbon nanotube	30	2.5	[40]
Fe_3O_4/graphene capsules	30	4.6	[41]
Fe@nanoporous carbon@ carbon fiber	25	5.2	[42]
Porous flower-like NiO@ graphene	25	4.2	[43]
Ni/Carbon nanocomposites	25	4.4	[44]
Graphene/NiO/PANI/Ag	70	4.9	[45]
Porous magnetic carbon	15	4.8	[46]
NiO/carbonized bamboo fibers	50	6.4	This work

https://doi.org/10.1021/acsomega.2c04767
ACS Omega 2022, 7, 39019−39027

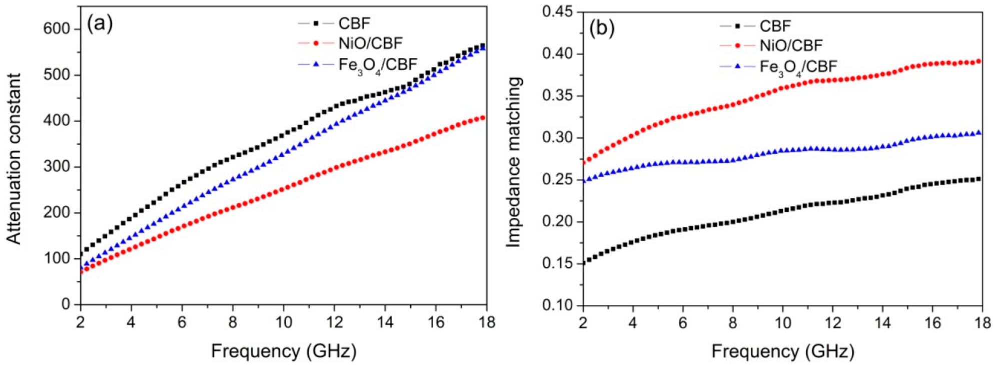

Figure 9. Attenuation constant (a) and characteristic impedance (b) of CBF, NiO/CBF, and Fe_3O_4/CBF.

absorption performance would become poor due to low electromagnetic loss. When increasing the filler content of NiO/CBF to 66.7 wt %, the microwave absorption performance was a little worse than that of NiO/CBF in the paraffin with 50 wt % due to inadequate impedance matching (see Supporting Information Figures S1−S3). Therefore, the excellent microwave absorption performance of NiO/CBF is attributed to appropriate complex permittivity, appropriate filler content, high impedance matching, and attenuation coefficient.

3. CONCLUSIONS

In summary, metal oxide/carbonized bamboo fibers derived from bamboo fibers were successfully fabricated by a feasible impregnation and subsequent calcination method. The dielectric component NiO and magnetic component Fe_3O_4 combined with carbonized bamboo fibers lead to appropriate complex permittivity, high impedance matching and attenuation coefficient, resulting in enhanced microwave absorption. Significantly, the NiO/carbonized bamboo fibers exhibit excellent microwave absorption performance in the entire X-band and Ku-band. This study is expected to provide a new strategy to design promising microwave absorption materials with the characteristics of low cost, lightweight, broadband, and easy mass production.

4. EXPERIMENTAL SECTION

Materials. Nickel nitrate ($Ni(NO_3)_2 \cdot 6H_2O$) and ferric nitrate ($Fe(NO_3)_3 \cdot 9H_2O$) were obtained from Tianjin Kaitong Chemical Reagent Co., Ltd. (Tianjin, China). The natural bamboo fiber used to prepare the carbonized bamboo fiber was purchased from Changchun Jiuli daily necessities Co., Ltd. (Changchun, China). High purity N_2 (Taiyuan Taineng Gas Co., Ltd., Taiyuan, China) was used as protective gas.

Preparation of NiO/Carbonized Bamboo Fibers. First, 10 g of natural bamboo fiber was carbonized in a tubular furnace at 700 °C for 2 h in a N_2 atmosphere with a heating rate of 4 °C/min to obtain carbonized bamboo fiber, named CBF. Then, after 0.8 g of carbonized bamboo fibers were immersed in $Ni(NO_3)_2$ solution (50 mL, 0.2 mol/L) for 24 h, the wet carbonized bamboo fibers were clamped out with tweezers. When there was no solution dripping, the wet carbonized bamboo fibers were put into an evaporation dish and dried at 60 °C for 10 h. Finally, the obtained $Ni(NO_3)_2$/carbonized bamboo fibers were calcined in a muffle furnace at 300 °C for 2 h to obtain NiO/carbonized bamboo fibers composites, named NiO/CBF.

Preparation of Fe_3O_4/Carbonized Bamboo Fibers. After 0.8 g of carbonized bamboo fibers were immersed in $Fe(NO_3)_3$ solution (50 mL, 0.2 mol/L) for 24 h, the wet carbonized bamboo fibers were clamped out with tweezers. When there was no solution dripping, the wet carbonized bamboo fibers were put into an evaporation dish and dried at 60 °C for 10 h. Finally, The obtained $Fe(NO_3)_3$/carbonized bamboo fibers were calcined in a muffle furnace at 300 °C for 2 h and subsequently calcined in a tubular furnace at 550 °C for 2 h in a N_2 atmosphere to obtain Fe_3O_4/carbonized bamboo fibers composites, named Fe_3O_4/CBF.

Characterization. The phase component was characterized by X-ray diffraction (XRD, XRD-6100). The morphology was characterized by JSM-7001F scanning electron microscope (SEM) with energy dispersion spectroscopy (EDS) and JEOL transmission electron microscopy (TEM). The Raman spectrum was measured by a Dxr2xi Raman spectrometer with a 532 nm laser. A LakeShore 7404 vibrating sample magnetometer (VSM) was used to measure the magnetic properties. STA6000 synchronous thermal analyzer was used for thermogravimetric (TG) analysis, and the temperature ranged from room temperature to 800 °C with a heating rate of 10 °C/min. The synthetic product was mixed with paraffin evenly with 50 wt % and made into a hollow ring sample in a concentric shaft mold (Φ_{out}= 7.0 mm, Φ_{in}= 3.0 mm). An Agilent N5224A vector network analyzer was used to measure the complex permittivity ε_r and the complex permeability μ_r in the frequency range of 2−18 GHz.

■ ASSOCIATED CONTENT

Supporting Information

The Supporting Information is available free of charge at https://pubs.acs.org/doi/10.1021/acsomega.2c04767.

Frequency dependence of complex permittivity, complex permeability, reflection loss, attenuation constant, and characteristic impedance for the absorbents with different mass percentages of NiO/CBF in paraffin (PDF)

■ AUTHOR INFORMATION

Corresponding Author

Wanxi Li − *Department of Materials Science and Engineering, Jinzhong University, Jinzhong 030619, P.R. China;* orcid.org/0000-0001-8100-8247; Email: liwanxi1986@163.com

Authors

Fang Guo — *Department of Materials Science and Engineering, Jinzhong University, Jinzhong 030619, P.R. China*

Yali Zhao — *Department of Materials Science and Engineering, Jinzhong University, Jinzhong 030619, P.R. China*

Yanyun Liu — *Department of Materials Science and Engineering, Jinzhong University, Jinzhong 030619, P.R. China*; orcid.org/0000-0001-7359-6739

Yien Du — *Department of Chemistry and Chemical Engineering, Jinzhong University, Jinzhong 030619, P.R. China*

Complete contact information is available at: https://pubs.acs.org/10.1021/acsomega.2c04767

Notes

The authors declare no competing financial interest.

■ ACKNOWLEDGMENTS

This work was supported by the Applied Basic Research Project of Shanxi (No. 20210302124045) and Shanxi Province Collaborative Innovation Center for Light Materials Modification and Application.

■ REFERENCES

(1) Zeng, X. J.; Cheng, X. Y.; Yu, R. H.; Stucky, G. D. Electromagnetic microwave absorption theory and recent achievements in microwave absorbers. *Carbon* **2020**, *168*, 606−623.

(2) Zhang, L. L.; Lv, Y. H.; Ye, X. Y.; Ma, L.; Chen, S.; Wu, Y. P.; Wang, Q. T. Polypyrrole Decorated Flower-like and Rod-like ZnO Composites with Improved Microwave Absorption Performance. *Materials* **2022**, *15*, 3408.

(3) Wang, F.; Gu, W. H.; Chen, J. B.; Wu, Y.; Zhou, M.; Tang, S. L.; Cao, X. Z.; Zhang, P.; Ji, G. B. The point defect and electronic structure of K doped $LaCo_{0.9}Fe_{0.1}O_3$perovskite with enhanced microwave absorbing ability. *Nano Res.* **2022**, *15*, 3720−3728.

(4) Li, X. L.; Yin, X. W.; Song, C. Q.; Han, M. K.; Xu, H. L.; Duan, W. Y.; Cheng, L. F.; Zhang, L. T. Self-Assembly Core-Shell Graphene-Bridged Hollow MXenes Spheres 3D Foam with Ultrahigh Specific EM Absorption Performance. *Adv. Funct. Mater.* **2018**, *28*, 1803938.

(5) Zhou, C. H.; Wu, C.; Liu, D.; Yan, M. Metal-Organic Framework Derived Hierarchical $Co/C@V_2O_3$ Hollow Spheres as a Thin, Lightweight, and High-Efficiency Electromagnetic Wave Absorber. *Chem. Eur. J.* **2019**, *25*, 2234−2241.

(6) Zhang, M.; Cao, M. S.; Shu, J. C.; Cao, W. Q.; Li, L.; Yuan, J. Electromagnetic absorber converting radiation for multifunction. *Mater. Sci. Eng. R* **2021**, *145*, 100627.

(7) Balci, O.; Polat, E. O.; Kakenov, N.; Kocabas, C. Graphene-enabled electrically switchable radar-absorbing surfaces. *Nat.Commun.* **2015**, *6*, 6628.

(8) Zhao, Y.; Hao, L. L.; Zhang, X. D.; Tan, S. J.; Li, H. H.; Zheng, J.; Ji, G. B. A Novel Strategy in Electromagnetic Wave Absorbing and Shielding Materials Design: Multi-Responsive Field Effect. *Small Sci.* **2022**, *2*, 2100077.

(9) Liang, L. L.; Gu, W. H.; Wu, Y.; Zhang, B. S.; Wang, G. H.; Yang, Y.; Ji, G. B. Heterointerface Engineering in Electromagnetic Absorbers: New Insights and Opportunities. *Adv. Mater.* **2022**, *34*, 2106195.

(10) Cao, M. S.; Shu, J. C.; Wen, B.; Wang, X. X.; Cao, W. Q. Genetic Dielectric Genes Inside 2D Carbon-Based Materials with Tunable Electromagnetic Function at Elevated Temperature. *Small Struct.* **2021**, *2*, 2100104.

(11) Estevez, D.; Qin, F. X.; Quan, L.; Luo, Y.; Zheng, X. F.; Wang, H.; Peng, H. X. Complementary design of nano-carbon/magnetic microwire hybrid fiber for tunable microwave absorption. *Carbon* **2018**, *132*, 486−494.

(12) Tian, K. H.; Wu, Y.; Shu, R. W.; Liu, Y.; Huang, Y. N.; Chen, Z. H.; Cheng, G. J. Facile synthesis of rod-like nickel cobaltite decorated reduced graphene oxide composites with excellent microwave absorption performance. *Mater. Lett.* **2021**, *295*, 129825.

(13) Wang, G. H.; Zhao, Y.; Yang, F.; Zhang, Y.; Zhou, M.; Ji, G. B. Multifunctional Integrated Transparent Film for Efficient Electromagnetic Protection. *Nano-Micro Lett.* **2022**, *14*, 65.

(14) Chen, X. T.; Zhou, M.; Zhao, Y.; Gu, W. H.; Wu, Y.; Tang, S. L.; Ji, G. B. Morphology control of eco-friendly chitosan-derived carbon aerogels for efficient microwave absorption at thin thickness and thermal stealth. *Green Chem.* **2022**, *24*, 5280−5290.

(15) Li, W. X.; Qi, H. X.; Guo, F.; Du, Y. E.; Song, N. J.; Liu, Y. Y.; Chen, Y. Q. Co nanoparticles supported on cotton-based carbon fibers: A novel broadband microwave absorbent. *J. Alloys Compd.* **2019**, *772*, 760−769.

(16) Shen, G. Z.; Ren, J. Z.; Zhao, B.; Mei, B. Q.; Wu, H. Y.; Fang, X. M.; Xu, Y. W. Magnetic hollow mesoporous carbon composites with impedance matching for highly effective microwave absorption. *J. Mater. Sci.* **2019**, *54*, 4024−4037.

(17) Yan, F.; Guo, D.; Zhang, S.; Li, C. Y.; Zhu, C. L.; Zhang, X. T.; Chen, Y. J. An ultra-small $NiFe_2O_4$ hollow particle/graphene hybrid: Fabrication and electromagnetic wave absorption property. *Nanoscale* **2018**, *10*, 2697−2703.

(18) Javid, M.; Qu, X. H.; Zhao, Y. P.; Huang, F. R.; Farid, A.; Zhang, H.; Shah, A.; Sammed, K. A.; Duan, Y. P.; Zhang, Z. D.; Pan, L. J.; Dong, X. L. Synthesis of hexagonal-shaped $Cr_3C_2@C$ nanoplatelets and role of their intrinsic properties towards microwave absorption. *Mater. Lett.* **2021**, *288*, 129329.

(19) Liu, J. L.; Zhang, L. M.; Wu, H. J. Enhancing the Low/Middle-Frequency Electromagnetic Wave Absorption of Metal Sulfides through F^- Regulation Engineering. *Adv. Funct. Mater.* **2022**, *32*, 2110496.

(20) Liu, J. L.; Zhang, L. M.; Wu, H. J. Anion-Doping-Induced Vacancy Engineering of Cobalt Sulfoselenide for Boosting Electromagnetic Wave Absorption. *Adv. Funct. Mater.* **2022**, *32*, 2200544.

(21) Liu, J. L.; Zhang, L. M.; Zang, D. Y.; Wu, H. J. A Competitive Reaction Strategy toward Binary Metal Sulfides for Tailoring Electromagnetic Wave Absorption. *Adv. Funct. Mater.* **2021**, *31*, 2105018.

(22) Wang, H. Y.; Zhang, Y. L.; Wang, Q. Y.; Jia, C. W.; Cai, P.; Chen, G.; Dong, C. J.; Guan, H. T. Biomass carbon derived from pine nut shells decorated with NiO nanoflakes for enhanced microwave absorption properties. *RSC Adv.* **2019**, *9*, 9126−9135.

(23) Yang, H. J.; Cao, M. S.; Li, Y.; Shi, H. L.; Hou, Z. L.; Fang, X. Y.; Jin, H. B.; Wang, W. Z.; Yuan, J. Enhanced Dielectric Properties and Excellent Microwave Absorption of SiC Powders Driven with NiO Nanorings. *Adv. Optical Mater.* **2014**, *2*, 214−219.

(24) Liu, P. J.; Ng, V. M. H.; Yao, Z. J.; Zhou, J. T.; Lei, Y. M.; Yang, Z. H.; Lv, H. L.; Kong, L. B. Facile Synthesis and Hierarchical Assembly of Flowerlike NiO Structures with Enhanced Dielectric and Microwave Absorption Properties. *ACS Appl. Mater. Interfaces* **2017**, *9*, 16404−16416.

(25) Xu, Z.; Wang, Z.; Wang, M. R.; Cui, H. T.; Liu, Y. Y.; Wei, H. Y.; Li, J. Large-scale synthesis of $Fe_9S_{10}/Fe_3O_4@C$ heterostructure as integrated trapping-catalyzing interlayer for highly efficient lithium-sulfur batteries. *Chem. Eng. J.* **2021**, *422*, 130049.

(26) Tu, C. Y.; Li, X.; Lu, C. C.; Luo, Q.; Li, T.; Zhu, M. Y. A sequential process to synthesize $Fe_3O_4@MnO_2$ hollow nanospheres for high performance supercapacitors. *Mater. Chem. Front.* **2022**, *6*, 1938−1947.

(27) Manna, R.; Srivastava, S. K. Reduced Graphene Oxide/Fe_3O_4/Polyaniline Ternary Composites as a Superior Microwave Absorber in the Shielding of Electromagnetic Pollution. *ACS Omega* **2021**, *6*, 9164−9175.

(28) Liang, X. H.; Quan, B.; Chen, J. B.; Gu, W. H.; Zhang, B. S.; Ji, G. B. Nano bimetallic@carbon layer on porous carbon nanofibers with multiple interfaces for microwave absorption applications. *ACS Appl. Nano Mater.* **2018**, *1*, 5712−5721.

(29) Liang, X. H.; Man, Z. M.; Quan, B.; Zeng, J.; Gu, W. H.; Zhang, Z.; Ji, G. B. Environment-Stable Co*x*Ni*y* Encapsulation in Stacked Porous Carbon Nanosheets for EnhancedMicrowave Absorption. *Nano-Micro Lett.* **2020**, *12*, 102.
(30) Zhang, B.; Du, Y. C.; Zhang, P.; Zhao, H. T.; Kang, L. L.; Han, X. J.; Xu, P. Microwave Absorption Enhancement of Fe_3O_4/Polyaniline Core/Shell Hybrid Microspheres with Controlled Shell Thickness. *J. Appl. Polym. Sci.* **2013**, *130*, 1909−1916.
(31) Xu, Q.; Wang, L. X.; Zhu, H. L.; Guan, Y. K.; Zhang, Q. T. Lightweight and efficient microwave absorbing materials based on walnut shell-derived nanoporous carbon. *Nanoscale* **2017**, *9*, 7408−7418.
(32) Cheng, Y.; Ji, G. B.; Li, Z. Y.; Lv, H. L.; Liu, W.; Zhao, Y.; Cao, J. M.; Du, Y. W. Facile synthesis of FeCo alloys with excellent microwave absorption in the whole Ku-band: Effect of Fe/Co atomic ratio. *J. Alloys Compd.* **2017**, *704*, 289−295.
(33) Liang, X. H.; Quan, B.; Man, Z. M.; Cao, B. C.; Li, N.; Wang, C. H.; Ji, G. B.; Yu, T. Self-assembly three-dimensional porous carbon networks for efficient dielectric attenuation. *ACS Appl. Mater. Interfaces* **2019**, *11*, 30228−30233.
(34) Li, W. X.; Liu, Y. Y.; Guo, F.; Du, Y. E.; Chen, Y. Q. Self-assembly sandwich-like Fe, Co, or Ni nanoparticles/reduced graphene oxide composites with excellent microwave absorption performance. *Appl. Surf. Sci.* **2021**, *562*, 150212.
(35) Che, R. C.; Peng, L. M.; Duan, X. F.; Chen, Q.; Liang, A. X. Microwave absorption enhancement and complex permittivity and permeability of Fe encapsulated within carbon nanotubes. *Adv. Mater.* **2004**, *16*, 401−405.
(36) Liu, P. J.; Yao, Z. J.; Ng, V. M. H.; Zhou, J. T.; Kong, L. B.; Yue, K. Facile synthesis of ultrasmall Fe3O4 nanoparticles on MXenes for high microwave absorption performance. *Composites Part A* **2018**, *115*, 371−382.
(37) Cao, M. S.; Song, W. L.; Hou, Z. L.; Wen, B.; Yuan, J. The effects of temperature and frequency on the dielectric properties, electromagnetic interference shielding and microwave-absorption of short carbon fiber/silica composites. *Carbon* **2010**, *48*, 788−796.
(38) Han, C.; Zhang, M.; Cao, W. Q.; Cao, M. S. Electrospinning and in-situ hierarchical thermal treatment to tailor C-$NiCo_2O_4$ nanofibers for tunable microwave absorption. *Carbon* **2021**, *171*, 953−962.
(39) Lü, Y. Y.; Wang, Y. T.; Li, H. L.; Lin, Y.; Jiang, Z. Y.; Xie, Z. X.; Kuang, Q.; Zheng, L. S. MOF-Derived Porous Co/C Nanocomposites with Excellent Electromagnetic Wave Absorption Properties. *ACS Appl. Mater. Interfaces* **2015**, *7*, 13604−13611.
(40) Zhang, M.; Song, S. N.; Liu, Y. M.; Hou, Z. X.; Tang, W. Y.; Li, S. N. Microstructural Design of Necklace-Like Fe_3O_4/Multiwall Carbon Nanotube (MWCNT) Composites with Enhanced Microwave Absorption Performance. *Materials* **2021**, *14*, 4783.
(41) Jian, X.; Wu, B.; Wei, Y. F.; Dou, S. X.; Wang, X. L.; He, W. D.; Mahmood, N. Facile synthesis of Fe_3O_4/GCs composites and their enhanced microwave absorption properties. *ACS Appl. Mater. Interfaces* **2016**, *8*, 6101−6109.
(42) Li, X.; Cui, E. B.; Xiang, Z.; Yu, L. Z.; Xiong, J.; Pan, F.; Lu, W. Fe@NPC@CFnanocomposites derived from Fe-MOFs/biomass cotton for lightweight and high-performance electromagnetic wave absorption applications. *J. Alloys Compd.* **2020**, *819*, 152952.
(43) Wang, L.; Xing, H. L.; Gao, S. T.; Ji, X. L.; Shen, Z. Y. Porous flower-like NiO@graphene composites with superior microwave absorption properties. *J. Mater. Chem. C* **2017**, *5*, 2005−2014.
(44) Xie, P. T.; Li, H. Y.; He, B.; Dang, F.; Lin, J.; Fan, R. H.; Hou, C. X.; Liu, H.; Zhang, J. X.; Ma, Y.; Guo, Z. H. Bio-gel derived nickel/carbon nanocomposites with enhanced microwave absorption. *J. Mater. Chem. C* **2018**, *6*, 8812−8822.
(45) Wang, Y.; Wu, X. M.; Zhang, W. Z.; Li, J. H.; Luo, C. Y.; Wang, Q. G. Fabrication and enhanced electromagnetic wave absorption properties of sandwich-like graphene@NiO@PANI decorated with Ag particles. *Synth. Met.* **2017**, *229*, 82−88.
(46) Zhao, H. Q.; Cheng, Y.; Lv, H. L.; Ji, G. B.; Du, Y. W. A novel hierarchically porous magnetic carbon derived from biomass for strong lightweight microwave absorption. *Carbon* **2019**, *142*, 245−253.
(47) Pan, H. X.; Yin, X. W.; Xue, J. M.; Cheng, L. F.; Zhang, L. T. In-Situ Synthesis of Hierarchically Porous and Polycrystalline Carbon Nanowires with Excellent Microwave Absorption Performance. *Carbon* **2016**, *107*, 36−45.
(48) Wang, S. S.; Jiao, Q. Z.; Liu, X. F.; Xu, Y. C.; Shi, Q.; Yue, S.; Zhao, Y.; Liu, H. B.; Feng, C. H.; Shi, D. X. Controllable Synthesis of γ-Fe_2O_3 Nanotube/Porous rGO Composites and Their Enhanced Microwave Absorption Properties. *ACS Sustainable Chem. Eng.* **2019**, *7*, 7004−7013.
(49) Liu, W.; Tan, S. J.; Yang, Z. H.; Ji, G. B. Enhanced Low Frequency Electromagnetic Properties of MOF-derived Cobalt through Interface Design. *ACS Appl. Mater. Interfaces* **2018**, *10*, 31610−31622.
(50) Ding, D.; Wang, Y.; Li, X. D.; Qiang, R.; Xu, P.; Chu, W. L.; Han, X. J.; Du, Y. C. Rational design of core-shell Co@C microspheres for high-performance microwave absorption. *Carbon* **2017**, *111*, 722−732.
(51) Liu, J. L.; Zhang, L. M.; Wu, H. J.; Zang, D. Y. Boosted electromagnetic wave absorption performance from vacancies, defects and interfaces engineering in $Co(OH)F/Zn_{0.76}Co_{0.24}S/Co_3S_4$ composite. *Chem. Eng. J.* **2021**, *411*, 128601.
(52) Guan, X. M.; Yang, Z. H.; Zhu, Y. T.; Yang, L. J.; Zhou, M.; Wu, Y.; Yang, L.; Deng, T. W.; Ji, G. B. The controllable porous structure and s-doping of hollow carbon sphere synergistically act on the microwave attenuation. *Carbon* **2022**, *188*, 1−11.
(53) Mu, Z. G.; Wei, G. K.; Zhang, H.; Gao, L.; Zhao, Y.; Tang, S. L.; Ji, G. B. The dielectric behavior and efficient microwave absorption of doped nanoscale $LaMnO_3$ at elevated temperature. *Nano Res.* **2022**, *15*, 7731−7741.